Preparation and Oxidation Performance of a NiCoCrAlYSiHf + NiAl Composite Coating Deposited by Arc Ion Plating and Magnetron Sputtering Techniques

Hongrui Yao, Chengyang Jiang, Zebin Bao, Shenglong Zhu, and Fuhui Wang

A NiCoCrAlYSiHf+NiAl composite coating was deposited onto a second-generation single-crystal superalloy René N5 by methods of arc ion plating and magnetron sputtering. After vacuum annealing, the composite coating exhibited a gradient distribution of elements, in which Al was enriched in outer layer and Cr was enriched in inner layer. Compared with conventional NiCoCrAlYSiHf and β-NiAl coatings, the composite coating was evaluated in isothermal and cyclic oxidation tests at 1100 °C in ambient air. The results showed that the oxidation rate of the composite coating was lower than that of NiCoCrAlYSiHf coating. Meanwhile, the extent of interdiffusion between coating and substrate in the composite coating was slighter compared with that in the β-NiAl coating. Microstructure evolutions of the composite coating after annealing and further oxidation test are investigated.

1. Introduction

MCrAlY (M = Ni and/or Co) coatings have been massively applied to gas turbine blades and other hot components offering reliable oxidation and corrosion resistances by the formation of dense and continuous oxide scales (mainly α-Al$_2$O$_3$), which can act as not only standalone overlay but also bondcoat (BC) within a thermal barrier coating system (TBCs) (Ref 1-4). However, at higher temperatures, e.g., 1100 °C, a rapidly growing thermally grown oxide (TGO) forms at the interface between the MCrAlY bondcoat and the top ceramic coating, resulting in crack propagation and ultimate failure of whole TBCs (the stress at the TGO/BC interface increases with the thickness of the TGO layer) (Ref 5-8). To further improve the oxidation performance, a quite number of studies have been carried out on the microstructure optimization and the composition modification of MCrAlY coatings (Ref 9-11).

Among the modified MCrAlY coatings by composition, the NiCoCrAlYSiHf coating series have drawn great attention for their excellent high-temperature oxidation and hot corrosion resistances. The addition of Hf to the coating is confirmed positive for reducing oxide growth rate and improving oxide scale adhesion, while Si addition benefits both oxidation and hot corrosion resistances (Ref 12-15). Even so, the lifetime and service temperature of NiCoCrAlYSiHf coating are still below expectation because of the relatively low Al content, since selective oxidation of Al only occurs on surface of a coating holding adequate Al content according to Wagner's theory (Ref 16). Theoretically, the Al concentration and activity in the coatings should be designed as high as possible in order to effectively extend the lifetime and improve the high-temperature oxidation resistance. However, simply increasing Al content in coating would step into a dilemma of deteriorating mechanical properties of substrate alloy, especially those single-crystal superalloys, by elements interdiffusion between coating and substrate.

Composite coatings designed by concepts of multi-layer or gradient structure have been put forward to solve the above-mentioned problems (Ref 17-21). Ren et al. (Ref 18) prepared a gradient coating consisting of inner magnetron-sputtered NiCrAlY coating and outer diffusion aluminized coating, which showed superior oxidation resistance at 1100 °C and exhibited excellent hot corrosion property in molten 75 wt.% Na$_2$SO$_4$ + 25 wt.% K$_2$SO$_4$/NaCl at 900 °C by forming continuous protective Al$_2$O$_3$ scales. Guo et al. (Ref 19, 20) prepared an Al/Cr gradient coating by combination of arc ion plating (AIP) and magnetron sputtering (MS), which also showed satisfied oxidation and hot corrosion resistances. Nicholls et al. (Ref 21) pointed out that smart coating was also a functionally gradient coating system with outer Al-rich

Hongrui Yao, Corrosion and Protection Division, Shenyang National Laboratory for Materials Science, Institute of Metal Research, Chinese Academy of Sciences, Shenyang 110016, China; and University of Chinese Academy of Sciences, Beijing 100049, China; **Chengyang Jiang**, Corrosion and Protection Division, Shenyang National Laboratory for Materials Science, Institute of Metal Research, Chinese Academy of Sciences, Shenyang 110016, China; and Corrosion and Protection Division, Shenyang National Laboratory for Materials Science, Northeastern University, Shenyang 110819, China; **Zebin Bao** and **Shenglong Zhu**, Corrosion and Protection Division, Shenyang National Laboratory for Materials Science, Institute of Metal Research, Chinese Academy of Sciences, Shenyang 110016, China; and **Fuhui Wang**, Corrosion and Protection Division, Shenyang National Laboratory for Materials Science, Northeastern University, Shenyang 110819, China. Contact e-mail: zbbao@imr.ac.cn.

layer and inner Cr-rich layer, which supplied protection over an extended range of service temperatures and corrosion environments that likely be experienced in an industrial gas turbine engine.

In our previous work, a microcrystalline β-NiAl coating prepared by MS could form a highly adherent α-Al$_2$O$_3$ scale with a low parabolic rate constant at 1100 °C, in which the constant was about 1/7 of NiCrAlY coating (Ref 22). However, the element interdiffusion between β-NiAl coating and the underlying substrate was very serious due to their conspicuous differences in chemical composition, which led to the formation of interdiffusion zone (IDZ) and secondary reaction zone (SRZ) after exposure to high temperatures. In order to improve the service life of MCrAlY coating and ameliorate the interdiffusion of β-NiAl coating simultaneously, a composite coating of β-NiAl over NiCoCrAlYSiHf was prepared by techniques of AIP and MS on René N5 superalloy in the present study. The microstructure evolution and high-temperature performance of the composite coating are investigated in comparison with conventional NiCoCrAlYSiHf and β-NiAl coatings. The research efforts are dedicated to investigate the oxidation mechanism and formation of various interdiffusion zones.

2. Experimental Procedures

2.1 Preparation of the Coatings

A second-generation Ni-base single-crystal superalloy Rene N5 bar was used as the substrate alloy in this study, whose nominal chemical composition (wt.%) is listed as follows: 7.5 Co, 7 Cr, 6.5 Ta, 6.2 Al, 5 W, 3 Re, 1.5 Mo, 0.15 Hf and balanced Ni. The specimens were cut in the form of disk with 15 mm in diameter and 2.2 mm in thickness. All the specimens were grounded down to 1000-grit SiC sandpaper, followed by ultrasonic cleaning in acetone and alcohol for individual 15 min.

NiCoCrAlYSiHf coating was prepared by means of AIP from a Ni-19Co-27Cr-11Al-0.5Y-0.1Si-0.2Hf (wt.%) alloy target. Prior to coating deposition, all the specimens were cleaned in vacuum by Ar$^+$ bombardment for 3 min at a bias voltage of $-$ 900 V to remove contaminant layer at surface and ensure good adhesion of coating. In deposition of NiCoCrAlYSiHf, the arc current was set at 70 A referring to a bias voltage of $-$ 50 V. Subsequently, the NiCoCrAlYSiHf-coated specimens were loaded into a MS facility for depositing microcrystalline β-NiAl, where the detailed deposition parameters have been described elsewhere (Ref 22). For comparison, a 27.8-µm-thick NiCoCrAlYSiHf coating and a 20.1-µm-thick β-NiAl coating were also prepared on René N5 substrate by AIP and MS using same deposition parameters, respectively. The chemical composition of as-deposited NiCoCrAlYSiHf coating detected by EDS is Ni-18Co-28Cr-19Al (at.%), while that of the as-deposited β-NiAl coating is Ni-52Al (at.%). Finally, all the specimens underwent vacuum annealing ($< 6 \times 10^{-3}$ Pa) treatment at 1000 °C for 4 h in a quartz tube furnace.

For convenience of discussion, the NiCoCrAlYSiHf + NiAl coating will be named as composite coating, while the simple NiCoCrAlYSiHf and β-NiAl coatings remain their original names hereafter.

2.2 High-Temperature Oxidation Tests

Isothermal oxidation tests were conducted at 1100 °C for 20 h in a thermal gravity analyzer (TGA, Thermax 700 thermal microbalance, Thermo Cahn, USA), with sensitivity of 10^{-5} g. After oxidation, each specimen was cooled to room temperature in the chamber of TGA.

Cyclic oxidation tests were carried out on the coated specimens using a vertical tube furnace equipped with automation ensuring specimens lifted up and down at regular intervals. In each cycle, the samples were exposed at 1100 °C for 1 h and then cooled in ambient air at room temperature for 10 min. The mass changes of specimens were measured using an electronic balance (Sartorius BP211D) with sensitivity of 0.01 mg after a certain number of cycles. For obtaining average mass change, three parallel specimens of each coating were used in the cyclic tests. To preserve oxide scales, the oxidized coating specimens for cross-sectional observation were deposited with a thin layer of electroless Ni-plating and mounted in resin.

2.3 Characterization

Surface and cross-sectional morphologies of the coatings were examined by scanning electron microscopy (SEM, Inspect F 50, FEI Co., Hillsboro, Oregon). Chemical compositions of the coatings were measured using either energy-dispersive spectrometer (EDS, X-Max, Oxford instruments Co., Oxford, UK) or electron probe microanalyzer (EPMA-1610, Shimadzu, Kyoto, Japan). Transmission electron microscopy (TEM, JEM-2100F, JEOL, Tokyo, Japan) was also used to investigate the detailed microstructure and elements distribution of the composite coatings. An x-ray diffractometer (XRD, X'Pert PRO, PANalytical Co., Almelo, Holland) was used for phase identification of the coatings.

3. Results and Discussion

3.1 Microstructure Evolution of the Composite Coating during Vacuum Annealing

Figure 1 shows surface and cross-sectional morphologies of the composite coating before and after vacuum annealing treatment. As can be seen from Fig. 1(c), the as-deposited coating comprised a β-NiAl top layer and a NiCoCrAlYSiHf bottom layer with thicknesses of 20.1 and 19.5 µm, respectively. The interfaces of NiAl/NiCoCrAlYSiHf and NiCoCrAlYSiHf/substrate were clear and well defined, indicating that there was bare interdiffusion during coating deposition due to the relatively low deposition temperature. The β-NiAl overlayer exhibited a typical cauliflower microstructure as shown in Fig. 1(a), and rare change was implemented after vacuum annealing at 1000 °C for 4 h (Fig. 1b). As to cross-sectional morphology, the composite coating became dense and the columnar microstructure almost disappeared after annealing (Fig. 1d). Besides, the original β-NiAl layer seemed to be thicker with a blurred NiAl/NiCoCrAlYSiHf interface, and an IDZ about 4.2 µm was formed below the composite coating after annealing.

Figure 2 shows x-ray diffraction results of NiCoCrAlYSiHf, β-NiAl and composite coatings after vacuum annealing. The NiCoCrAlYSiHf coating consists of β, γ/γ′, α-Cr and σ-(Cr, Co, Ni) phases, while β-NiAl coating merely comprised β
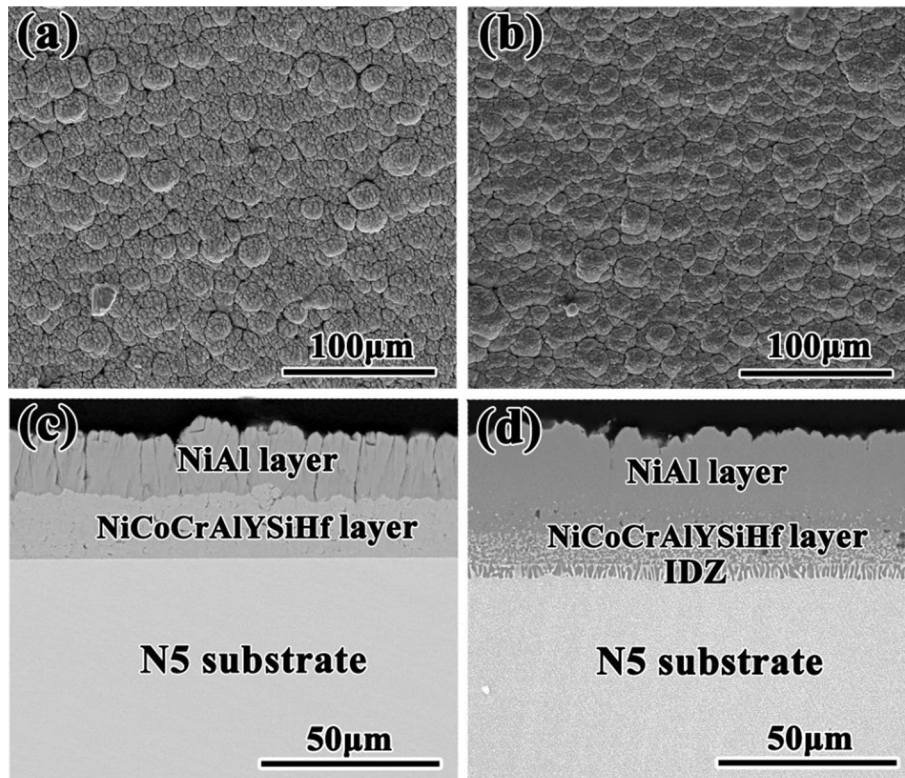
Fig. 1 Surface and cross-sectional morphologies of as-prepared (a and c) and as-annealed (b and d) composite coatings
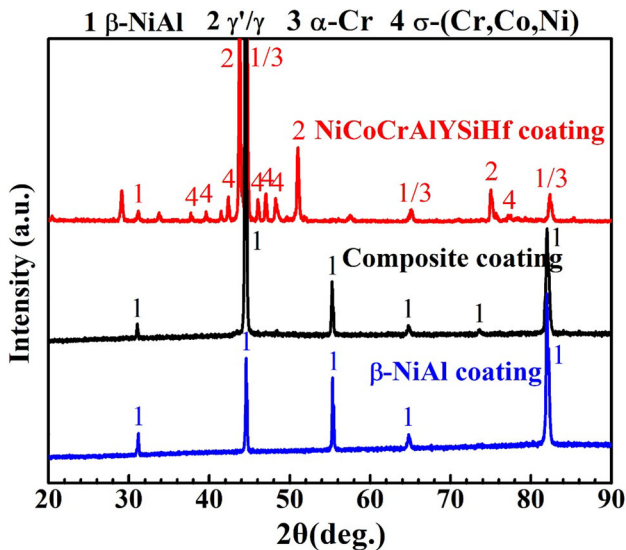

Fig. 2 XRD patterns of NiCoCrAlYSiHf, composite and β-NiAl coatings after vacuum annealing

phase. For the composite coating, only β phase was reflected due to depth limitation of XRD test.

Figure 3 displays the STEM images and the corresponding EDS mappings of interfacial zones of the as-annealed composite coating. According to Fig. 3(a), the elements near the interface of NiAl/NiCoCrAlYSiHf were distributed homogeneously except for Cr, in which Cr-rich particles were segregated in the both sides after annealing. As shown in Fig. 3(b), interdiffusion of elements occurred between composite coating and alloy substrate, forming a 4.2-μm-thick IDZ

in the substrate, which consisted of β matrix and fine topologically close-packed (TCP) phases enriched with refractory elements (e.g., Re, W and Mo).

The quantitative elemental concentration results (by EPMA) from the top surface to the interior of coating for the as-annealed composite coating are shown in Fig. 4. Clearly, the as-annealed composite coating comprised a 25.1-μm-thick Al-rich outer layer and a 15.9-μm-thick Cr-rich inner layer. The outer Al-rich region increased in thickness compared with the original β-NiAl layer, while the thickness of inner NiCoCrAlYSiHf layer decreased after annealing, which is consistent with the results of SEM image shown in Fig. 1(d). A fluctuation of elements concentration at the inner layer of the composite coating can be observed due to passage of scanning spots over different phases by EPMA.

In the procedure of vacuum annealing, interdiffusion of elements occurred at both NiAl/NiCoCrAlYSiHf and NiCoCrAlYSiHf/substrate interfaces. In order to further elaborate the interdiffusion process, the schematic of microstructure evolution of the composite coating during vacuum annealing treatment is illustrated in Fig. 5. In the outer β-NiAl layer, Ni and Al diffused inwardly to the NiCoCrAlYSiHf layer while Co and Cr diffused to the opposite direction, in which the outer β-NiAl layer became dense due to the lattice expansion induced by phase evolution from Al-rich β-NiAl (52 at.% Al) to Ni-rich β-NiAl (53 at.% Ni). As the interdiffusion continued, the reaction of Al and Ni contributed to the growth of β phases along NiAl/NiCoCrAlYSiHf interface. (A considerable amount of γ/γ′ had changed to Ni-rich β-NiAl.) The original NiAl/NiCoCrAlYSiHf interface became unclear, and the Al-rich outer layer (dominated with Ni-rich β-NiAl) of the composite coating became thicker than the original β-NiAl layer. Besides, Cr-rich phases, such as α-Cr and σ-(Cr, Co, Ni), were
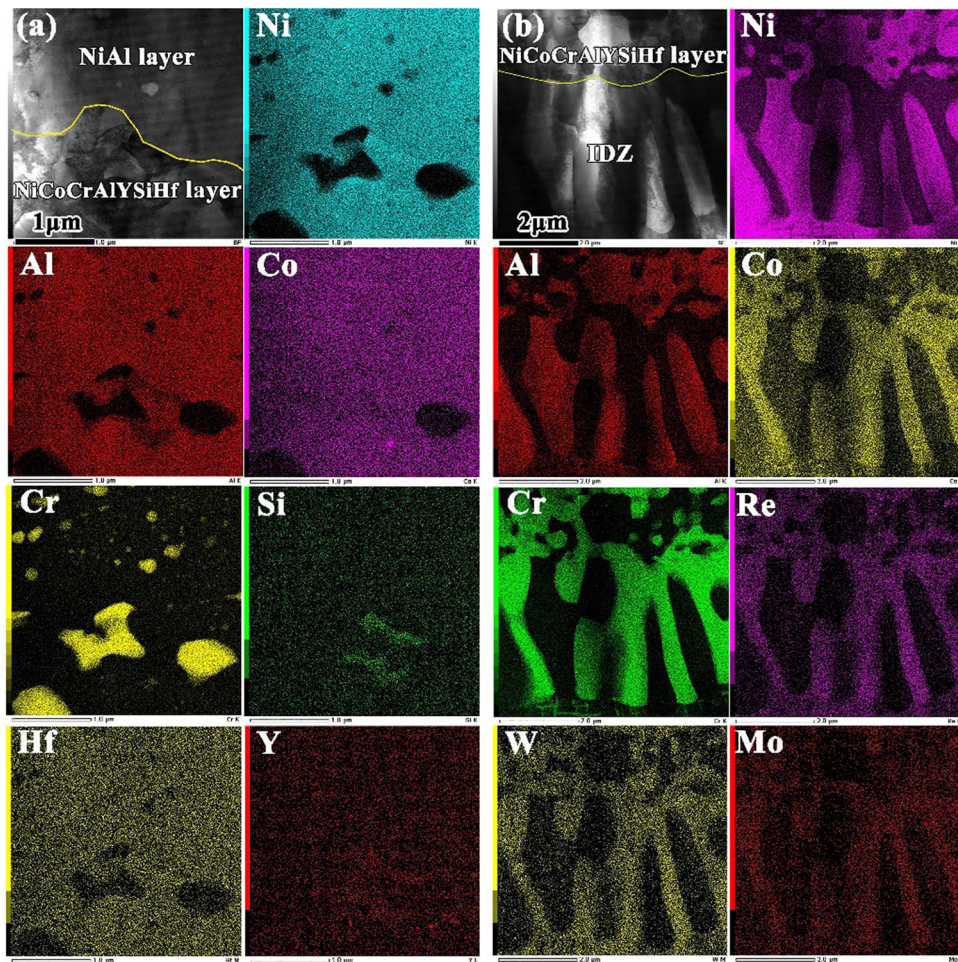
Fig. 3 STEM images and the corresponding EDS mappings characterized on the as-annealed composite coating: NiAl/NiCoCrAlYSiHf interface (a) and NiCoCrAlYSiHf/substrate interface (b)
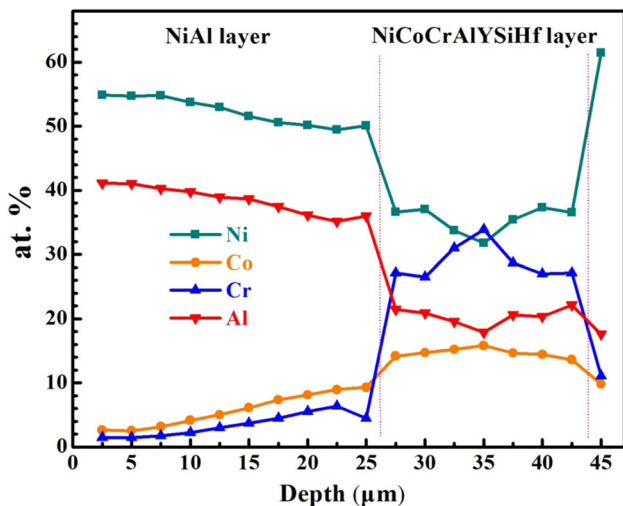
Fig. 4 Element distributions of the as-annealed composite coating measured by EPMA

precipitated within the NiCoCrAlYSiHf layer after vacuum annealing because the solubility of Cr in β phases was much lower than that in γ/γ' phases (Ref 23-25).

Furthermore, the composition gradient between composite coating and alloy substrate also provided the driving force for coating/substrate interdiffusion during high-temperature annealing, which enhanced the adhesion between the coating and the substrate. On the other hand, the diffusion fluxes of Al from the composite coating and Ni from the alloy substrate implemented phase transformation from γ/γ' to β in the substrate. Because of the low solubility of refractory metals (such as Re, W and Mo) in β, and the diffusion mobility of these elements in Ni-base superalloy is much slower than Ni and Al (Ref 26), in which an in situ precipitation of Re, W and Mo could occur forming TCP particles in IDZ (see Fig. 5). In beginning, the as-precipitated TCP particles in IDZ are quite fine, but they will congregate and grow to notable large size after further exposure at high temperatures (Ref 27, 28).

3.2 Isothermal Oxidation Kinetics of the Coatings

The isothermal oxidation kinetics of NiCoCrAlYSiHf, composite and β-NiAl coatings at 1100 °C in ambient air are shown in Fig. 6. As presented in Fig. 6(a), all coatings exhibited significant mass gains in the initial oxidation stage, which resulted from the fast formation of oxide scales on the surface. As the oxidation time increased, the three coatings showed similar tendency and the oxidation rates of the steady stage were all basically in accordance with the parabolic
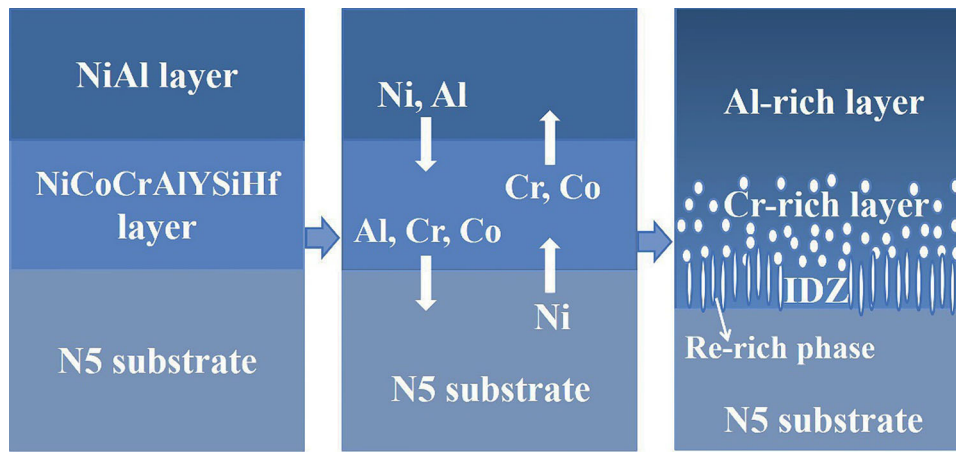
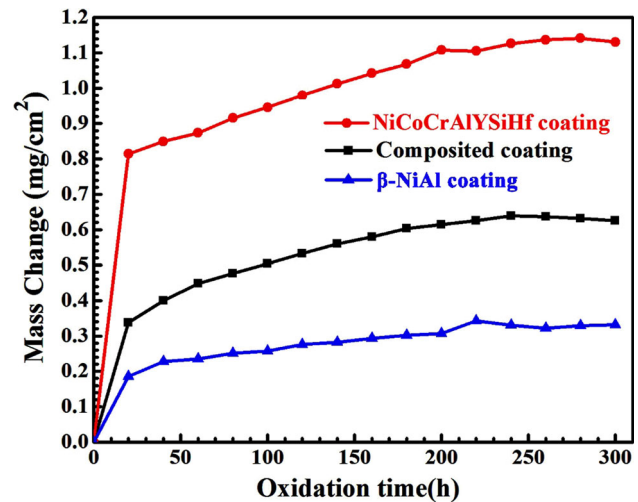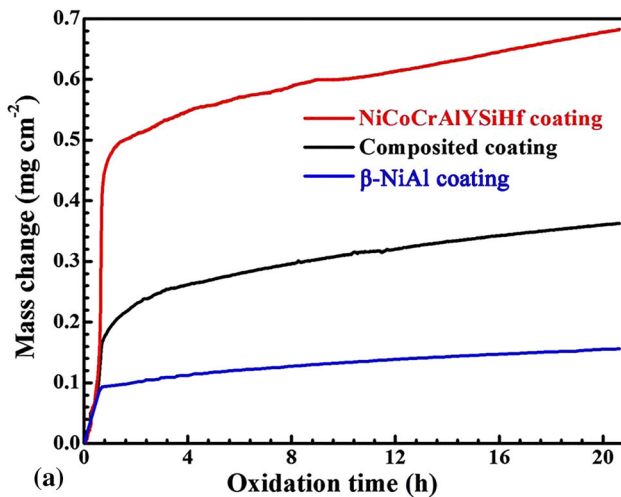**Fig. 5** Schematics showing microstructure evolution of the composite coating during vacuum annealing treatment

(a)

(b)

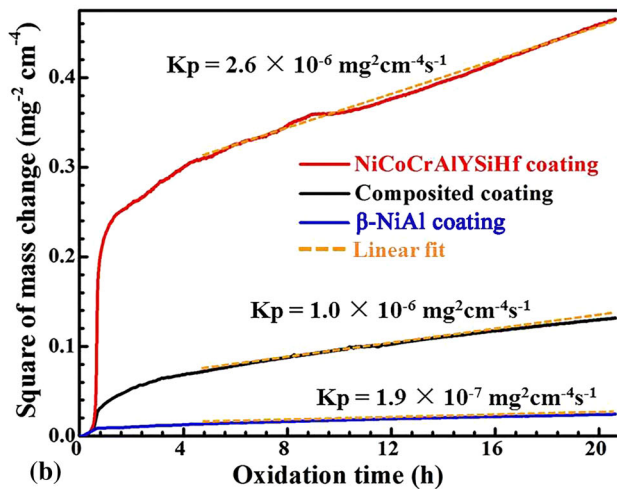**Fig. 6** Isothermal oxidation kinetics curves of NiCoCrAlYSiHf, composite and β-NiAl coatings at 1100 °C in air: y vs. t (a) and y^2 vs. t (b)

kinetics. Therefore, the mass gains of these coatings as a function of the oxidation time were approximately in conformity with the following equation:

$$(\Delta w)^2 = K_p \cdot t$$

Fig. 7 Cyclic oxidation kinetic curves of the NiCoCrAlYSiHf, composite and β-NiAl coatings at 1100 °C in air

where Δw is the mass gain of unit area, K_p is the parabolic oxidation rate constant and t is the oxidation time in hour (Ref 29). Through the above ground, the oxidation of all coatings comprised a fast oxide scale-forming stage and a stable growing stage that normally obeyed the parabolic kinetics. Thus, data in stable stage ($t \geq 5$ h) were selected for fitting the oxidation kinetics, and the specific K_p values of various coatings calculated from the fitting curves in Fig. 6(b) were presented. As indicated, the K_p value for NiCoCrAlYSiHf coating (2.6×10^{-6} mg^2 cm^{-4} s^{-1}) was about 2.6 times of that for the composite coating (1.0×10^{-6} mg^2 cm^{-4} s^{-1}), indicating that the composite coating reduced the oxidation rate significantly. However, pure β-NiAl coating exhibited the lowest oxidation rate ($K_p = 1.9 \times 10^{-7}$ mg^2 cm^{-4} s^{-1}) than both the NiCoCrAlYSiHf and composite coatings.

3.3 Cyclic Oxidation Behavior of the Coatings

3.3.1 Oxidation Products and Morphologies. Figure 7 shows the mass change curves of NiCoCrAlYSiHf, composite and β-NiAl coatings during cyclic oxidation at 1100 °C in air.

Similar trend of mass gain as parabolic law in consistent with isothermal oxidation was observed from all the coatings. After oxidation for 300 cycles, the mass gain of NiCoCrAlYSiHf coating was 1.13 mg/cm^2 while it was 0.33 mg/cm^2 for the β-NiAl coating. Compared to the other two coatings, the mass gain of composite coating was 0.63 mg/cm^2, nearly twice of that of the β-NiAl coating but half of that of NiCoCrAlYSiHf coating.

Figure 8 shows the XRD patterns of the three coatings after cyclic oxidation at 1100 °C for 300 cycles in air. Mixed oxides consisting of α-Al$_2$O$_3$, Co$_2$CrO$_4$ and NiAl$_2$O$_4$ were formed on NiCoCrAlYSiHf coating, while the oxide scales formed on both composite and β-NiAl coatings were exclusively composed of α-Al$_2$O$_3$. However, the degeneration of β to γ/γ′ occurred in all coatings by the diffraction peaks of γ/γ′ phases.

Figure 9 displays the surface and cross-sectional morphologies of NiCoCrAlYSiHf, composite and β-NiAl coatings after cyclic oxidation at 1100 °C for 300 cycles in air. Large spallation zones on the surface of NiCoCrAlYSiHf coating were observed from the surface morphology shown in Fig. 9(a). It can also be noticed from the corresponding cross-sectional morphologies in Fig. 9(d) that a thick bilayer oxide scale (outer mixed oxides in light gray and the inner α-Al$_2$O$_3$ layer in dark) was formed on the surface. The average Al content in the NiCoCrAlYSiHf coating decreased to 3.33 wt.% according to EDS analysis. Another noticeable phenomenon was that the oxide scale of NiCoCrAlYSiHf coating rumpled seriously, which could be induced by the volume change accompanied with phase transformation from β + γ/γ′ to γ. According to Y.F. Yang et al. (Ref 30), the rumpling of the coating and oxide scale should partly be attributed to oxide scale spallation. In addition, the IDZ and SRZ with an overall depth of 56.4 μm formed beneath the NiCoCrAlYSiHf coating, where the TCP phases dispersed homogeneously.

In comparison with NiCoCrAlYSiHf coating, thin and single oxide scales formed on both composite and β-NiAl coatings (Fig. 9e and f) as well as there was little spallation occurred on the surface after cyclic oxidation at 1100 °C for 300 cycles (Fig. 9b and c). The difference in the thickness of

the oxide scales forming on these two coatings was very small, which confirmed that the differences of oxidation kinetics for these two coatings in Fig. 6 may be accounted for other reasons. As a matter of fact, the geometry roughness of the composite coating prepared by AIP was larger than that of the sputtered β-NiAl coating, which caused that the effective surface area for the composite coating was much larger than the expectation because we generally regarded the surface area as an ideal coupon to calculate the mass gain of unit area (Ref 31). In addition, the most evident advantages of the composite coating in comparison with β-NiAl coatings were the relieved coating degradation rate and the interdiffusion extent. In Fig. 9(e), the outer Al-rich layer in the composite coating degraded into β + γ′ layer and the inner NiCoCrAlYSiHf layer degraded into γ′ layer after 300 1-h cycles tests at 1100 °C. According to EDS analysis, the average Al contents in both layers were 17.1 wt.% and 8.1 wt.%, respectively. During cyclic oxidation, all the β phases in original IDZ have converted into γ′ phases due to the further inward diffusion of Al to substrate, as well as the fine precipitates in IDZ gathered and became coarser. After 300 cycles, the IDZ in composite coating system became undistinguishable and a 29.8-μm-thick SRZ with needle-like TCP precipitates formed beneath the IDZ. The pure β-NiAl coating, just as shown in Fig. 9(f), has degraded into upper (above the red dash line) and lower (beneath the red dash line) sub-layers, which could be referred to Al-deficient β-NiAl and γ′-Ni$_3$Al phases. Some isolated γ′-Ni$_3$Al phase zones were also formed in the upper sub-layer as Al diffused outwardly to form oxide scale during long-term cyclic exposure at 1100 °C. The average Al contents in upper and lower sub-layers were 20.1 wt.% and 11.8 wt.%, respectively, according to EDS analysis. Besides, a 9.3-μm-thick IDZ and a 58.9-μm-thick SRZ formed under the β-NiAl coating, with some round- and needle-shaped TCPs. Visible Kirkendall holes were generated at the coating/substrate interface due to the unbalanced interdiffusion of elements.

3.3.2 Elements Interdiffusion Characterized by EPMA Mapping. The EPMA mapping for NiCoCrAlYSiHf coating in Fig. 10 displayed that the bilayer oxide scale contained Ni, Co, Cr, Al and O in the upper layer and was rich in Al and O in the subsequent layer. Combined with the XRD patterns in Fig. 8, it confirmed that the outer layer of oxide scale in NiCoCrAlYSiHf coating was mainly spinel oxides, such as Co$_2$CrO$_4$ and NiAl$_2$O$_4$, while the inner layer was primarily α-Al$_2$O$_3$. Beneath the surface oxide scale, a large Al-depleted zone formed, which referred to the degraded coating and the adjacent substrate. The inward diffusion of Cr and Co was not surprising because of the chemical potential discrepancy between coating and substrate, so the concentration of Cr and Co in the substrate neighboring to coating was higher than that in the deeper substrate. The high diffusion flux of Cr from coating to substrate can not be completely solid-dissolved in γ/γ′ phases, as a result part of Cr combined with the refractory elements (such as Re) to form TCP phases (Ref 32-34).

Similar to that in Fig. 9(e), some large Al-depleted zones in the outer β-NiAl layer of composite coating are observed in Fig. 11, which were the degraded γ′-Ni$_3$Al phases due to Al consumption from the coating to form the surface oxide scale. Beneath this layer (the original NiCoCrAlYSiHf layer in the composite coating), an intriguing phenomenon could be observed from the element distribution after oxidation. Firstly, the concentration of Co was high in this layer in contrast to the adjacent substrate. Co atoms seemed to diffuse from substrate
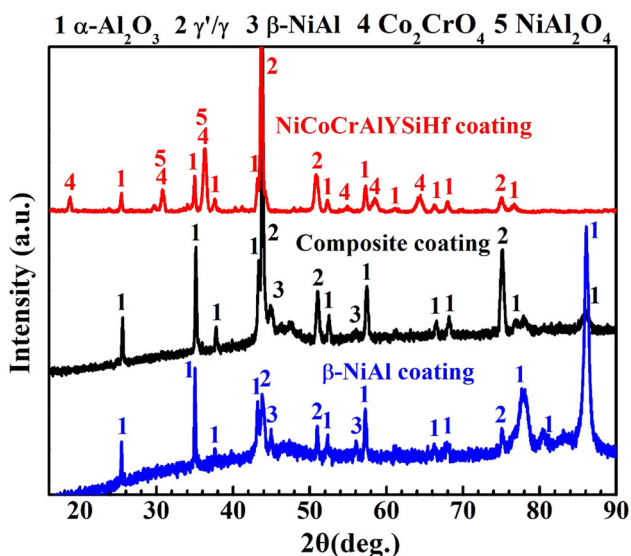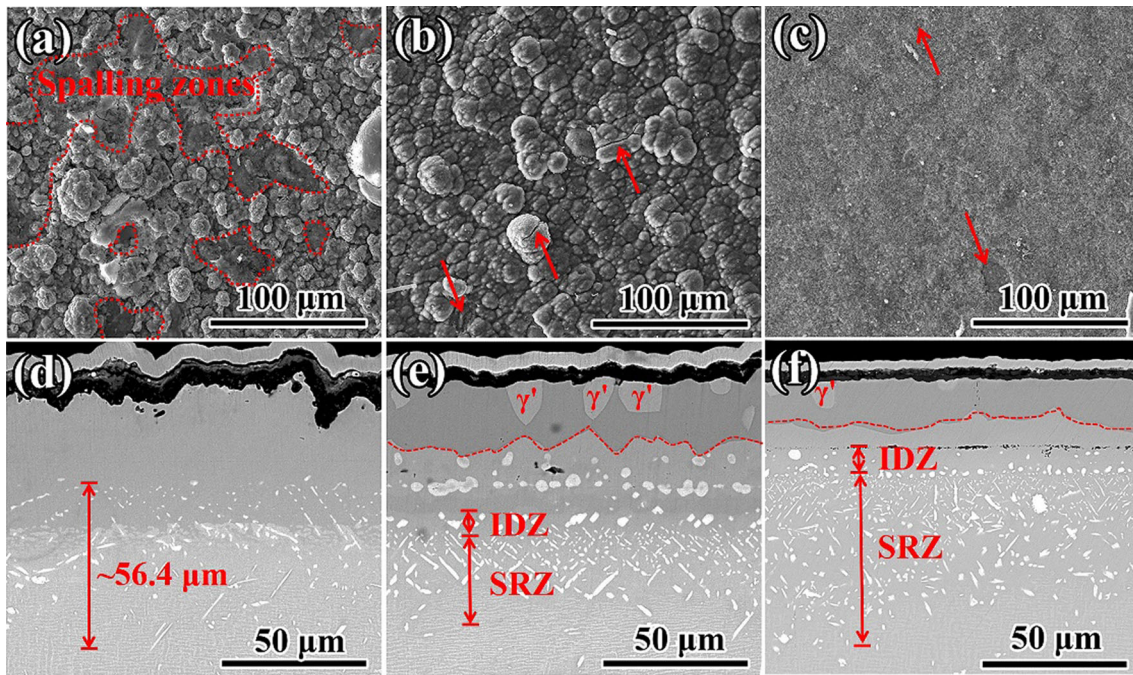
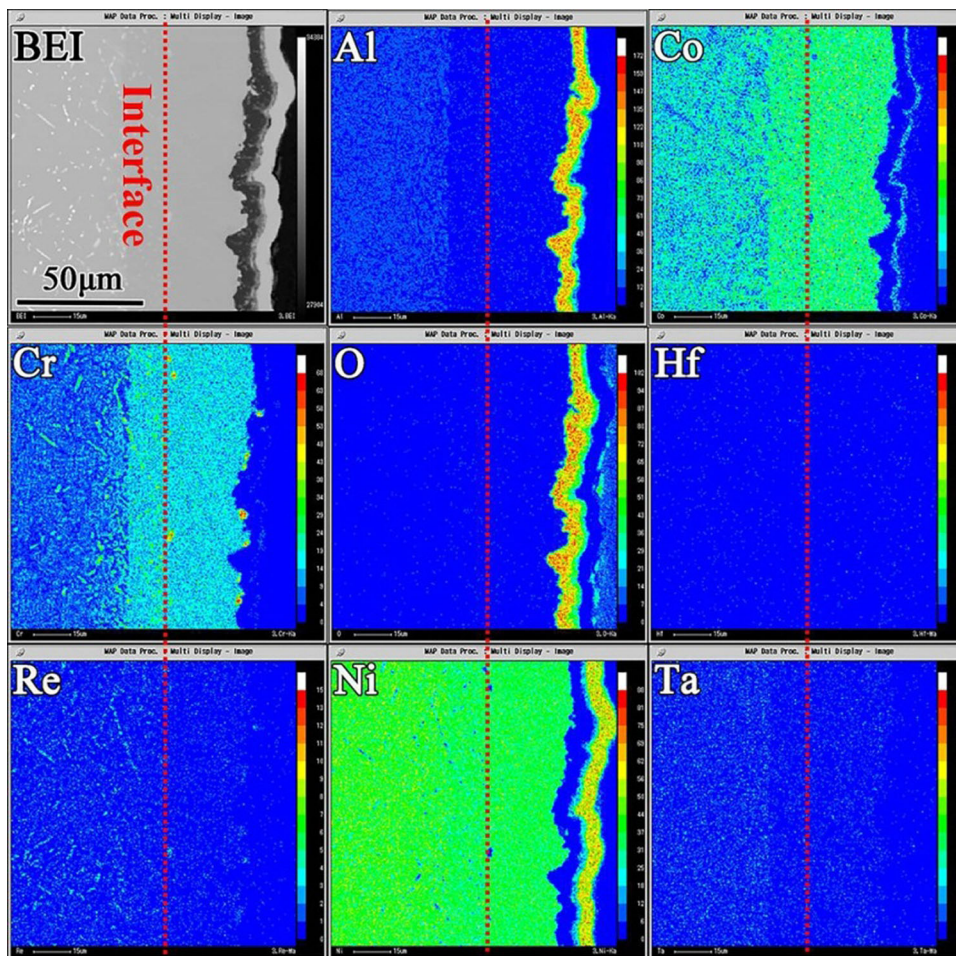**Fig. 8** XRD patterns of NiCoCrAlYSiHf, composite and β-NiAl coatings after cyclic oxidation at 1100 °C for 300 cycles in air

Fig. 9 Surface and cross-sectional morphologies of NiCoCrAlYSiHf (a, d), composite (b, e) and β-NiAl (c, f) coatings after cyclic oxidation at 1100 °C for 300 cycles in air

Fig. 10 Elemental mappings for the NiCoCrAlYSiHf coating after cyclic oxidation at 1100 °C for 300 cycles in air
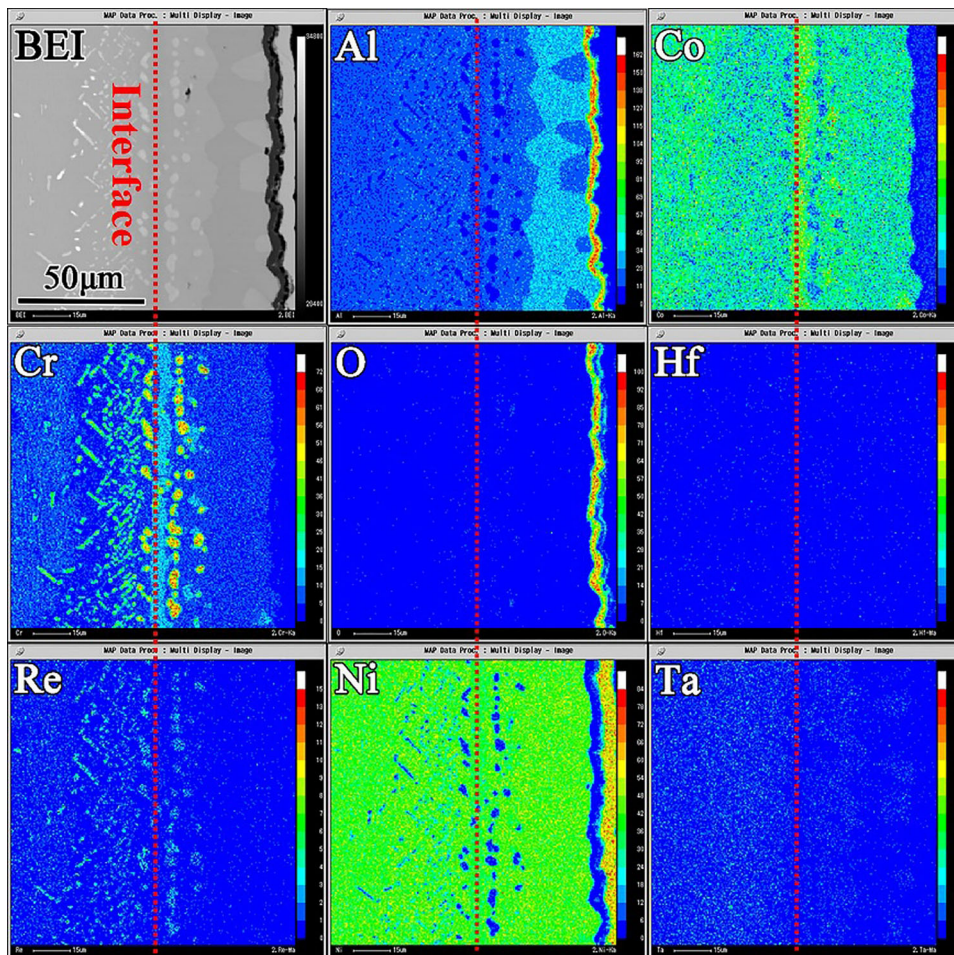
Fig. 11 Elemental mappings for the composite coating after cyclic oxidation at 1100 °C for 300 cycles in air

to coating and got enriched there, which was exactly the opposite direction for concentration gradient, so an uphill diffusion must exist. The mechanism for the uphill diffusion of Co may be associated with the $\gamma/\gamma' \rightarrow \gamma'$ reaction in the substrate during oxidation. (Co possesses lower solubility in γ' phase.) Secondly, the Cr distributed throughout this layer but it was not even, part of it overlapping with Re in upper sub-layer and others segregating together into a continuous Cr-rich zone in lower sub-layer. As expected, there was relatively low Al content in the Cr-rich zone. In addition, precipitations of Re overlapped with Cr in both IDZ and SRZ, and most of Ta existed in the γ' phases.

The mapping for pure β-NiAl coating after 300 1-h cycles at 1100 °C in air is shown in Fig. 12. There was an Al-rich layer right beneath the alumina scale, which was the outer part of β-NiAl coating. Co diffused from the substrate throughout the whole coating. Segregation of Cr occurred in IDZ and SRZ, while a little amount of Cr could be detected in the coating. Re presence overlapped with the Cr-rich phases. Ta mainly existed in the coherent γ' zones, although regional enrichment could be observable.

It is well known that there are two ways for Al to be consumed in high-temperature protective coatings during service. One is the consumption by alumina scale growth and reparation, and the other is the meaninglessly inward diffusion to substrate. At the beginning, the two ways take place simultaneously. However, once a dense and protective alumina

scale forms on the surface of coating, the alumina scale can effectively inhibit the ingress of oxygen and then reduce the consumption rate of Al. Therefore, the interdiffusion between coating and substrate plays a primary role in the degradation of the protective coatings during the long-time oxidation, especially coating with high Al content. Interdiffusion of elements between coating and substrate will bring out the next problems. Firstly, the Kirkendall voids formed in the interface of coating/substrate are detrimental to the coating adhesion (Ref 35). Secondly, the Al content in the coating decreases because of inward diffusion to the substrate, which increases degradation rate and reduces the lifetime of coatings (Ref 36-38). Finally, the formation of TCP phases and SRZ could seriously deteriorate the ductility and creep resistance of Ni-base superalloys, especially for single-crystal superalloys (Ref 39-41).

In this work, the low Al content in NiCoCrAlYSiHf coating was far below the critical Al content for exclusive alumina scale formation and reparation at 1100 °C or above. Mixed oxides including spinel formed on the surface of NiCoCrAlYSiHf coating, and the average Al content in the coating decreased to 3.33 wt.% (by EDS) after cyclic oxidation test (Fig. 9d and Fig. 10). Therefore, it can be inferred that the primary way for Al consumption in NiCoCrAlYSiHf coating is the alumina scale growth and reparation in this study. However, there is adequate Al content for the formation of single protective alumina scale in the cases of both composite and β-NiAl
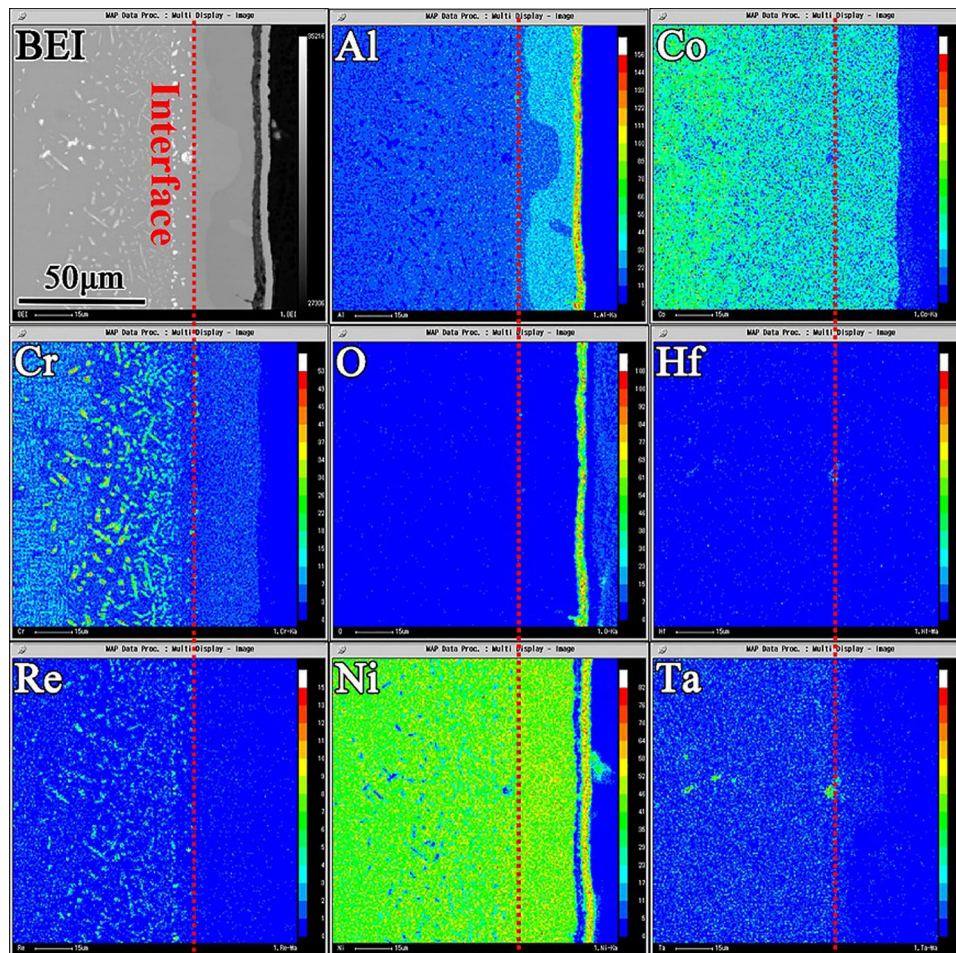
Fig. 12 Elemental mappings for the β-NiAl coating after cyclic oxidation at 1100 °C for 300 cycles in air

coatings (Fig. 9e and f). So, the primary way for Al to be consumed in these two coatings is the inward diffusion from the coating to the substrate during long-time oxidation, which led to the formation of IDZ and SRZ. A comprehensive interdiffusion model for SRZ formation in β-NiAl-coated single-crystal superalloy is proposed in our previous work (Ref 31), which illustrates that the SRZ formation is driven by coating and alloy composition, crystal orientation and residual stress introduced by the surface finishing under a precondition that the interdiffusion flux is too low to sustain the $\gamma/\gamma' \rightarrow \beta$ reaction at the IDZ/substrate interface. In this work, the conditions for SRZ formation were satisfied in both composite and β-NiAl coatings during cyclic oxidation tests, but the thickness of SRZ in composite coating was only half of that in β-NiAl coating. This demonstrated the SRZ growth kinetics in both coatings were different. Matsuoka et al. (Ref 42) calculated the diffusion coefficients and activation energy from the SRZ growth kinetics in a pack-cemented fourth-generation superalloy TMS-138 and found that they are very similar to the data for Al diffusion in γ'-Ni_3Al. Combined with the results in Fig. 9(e) and Fig. 11, it can be speculated that the NiCoCrAlYSiHf layer in composite coating exhibited certain buffering and inhibitory effects on the growth of SRZ. Firstly, the addition of NiCoCrAlYSiHf layer increased the distance of Al diffusion flux from β-NiAl layer to substrate, which was an important factor in determining the rate that Al can be effectively transported into the substrate (Ref

43). Secondly, it is known that Co and Cr were preferentially partitioned to the γ phase in Ni-base superalloy. Therefore, for the β-NiAl coating system, the inward diffusion of Al and outward diffusion of Co and Cr tended to make the γ phase in the γ/γ' substrate instable, causing the formation of SRZ. On the contrary, for the composite coating system, the addition of NiCoCrAlYSiHf layer could act as a buffering layer to slow down inward diffusion of Al and outward diffusion of Co/Cr from substrate, which could stabilize the γ/γ' coherent structure in superalloy and then retard the growth of SRZ effectively. Finally, the continuous Cr-rich zone in the inner layer may be responsible for the slow growth of SRZ because the Al content in this layer was quite low, which led to the low diffusion rate of Al through this layer. Somehow, further investigation is needed for the aim to explore the mechanism of the slow growth of SRZ in the composite coating at a deeper insight.

4. Conclusions

The composite coating presented a compromised property: slighter interdiffusion extent and much enhanced oxidation resistance, which combined advantages of NiCoCrAlYSiHf and β-NiAl coatings together. According to the experimental results, following conclusions can be drawn:

(1) A NiCoCrAlYSiHf + NiAl composite coating was deposited on single-crystal superalloy René N5 by arc ion plating and magnetron sputtering. After vacuum annealing, the composite coating showed a gradient distribution, which comprised Al-rich outer layer and Cr-rich inner layer.

(2) Compared with NiCoCrAlYSiHf coating, the composite coating exhibited good oxidation resistance at 1100 °C. The K_p value for composite coating was less than two-fifths of that for NiCoCrAlYSiHf coating during isothermal oxidation. Exclusive α-Al_2O_3 formed on the composite coating, while mixed oxides of spinel and α-Al_2O_3 formed on the NiCoCrAlYSiHf coating after cyclic oxidation at 1100 °C for 300 h.

(3) The thickness of SRZ in case of composite coating was nearly half of that in β-NiAl coating because the NiCoCrAlYSiHf layer in composite coating exhibited certain inhibitory effects on the growth of SRZ.

References

1. N.P. Padture, M. Gell, and E.H. Jordan, Thermal Barrier Coatings for Gas-Turbine Engine Applications, *Science*, 2002, **296**, p 280–284

2. T.N. Rhys-Jones, Coatings for Blade and Vane Applications in Gas Turbines, *Corros. Sci.*, 1989, **29**, p 623–646

3. W. Brandl, H.J. Grabke, D. Toma, and J. Kruger, The Oxidation Behaviour of Sprayed MCrAlY Coatings, *Surf. Coat. Technol.*, 1996, **86–87**, p 41–47

4. C. Leyens, K. Fritscher, R. Gehrling, M. Peters, and W.A. Kaysser, Oxide Scale Formation on an MCrAlY Coating in Various H2-H2O Atmospheres, *Surf. Coat. Technol.*, 1996, **82**, p 133–144

5. D. Naumenko, V. Shemet, L. Singheiser, and W.J. Quadakkers, Failure Mechanisms of Thermal Barrier Coatings on MCrAlY Type Bondcoats Associated with the Formation of the Thermally Grown Oxide, *J. Mater. Sci.*, 2009, **44**, p 1687–1703

6. Y.J. Li, Y.T. Xie, L.P. Huang, X.Y. Liu, and X.B. Zheng, Effect of Physical Vapor Deposited Al_2O_3 Film on TGO Growth in YSZ/CoNiCrAlY Coatings, *Ceram. Int.*, 2012, **38**, p 5113–5121

7. D. Renusch, M. Schorr, and M. Schutze, The Role that Bond Coat Depletion of Aluminum has on the Lifetime of APS-TBC Under Oxidizing Conditions, *Mater. Corros.*, 2008, **59**, p 547–555

8. P. Niranatlumpong, C.B. Ponton, and H.E. Evans, The Failure of Protective Oxides on Plasma-Sprayed NiCrAlY Overlay Coatings, *Oxid. Met.*, 2000, **53**, p 241–258

9. M.L. Shen, P.P. Zhao, Y. Gu, S.L. Zhu, and F.H. Wang, High Vacuum Arc Ion Plating NiCrAlY Coatings: Microstructure and Oxidation Behavior, *Corros. Sci.*, 2015, **94**, p 294–304

10. Y.N. Wu, M. Qin, Z.C. Feng, Y. Liang, C. Sun, and F.H. Wang, Improved Oxidation Resistance of NiCrAlY Coatings, *Mater. Lett.*, 2003, **57**, p 2404–2408

11. Y.N. Wu, Q.M. Wang, P.L. Ke, C. Sun, J. Gong, F.H. Wang, and L.S. Wen, Evaluation of arc ion plated NiCoCrAlYSiB Coatings after Oxidation at 900–1000 °C, *Surf. Coat. Technol.*, 2006, **200**, p 2857–2863

12. K.A. Unocic and B.A. Pint, Characterization of the Alumina Scale Formed on a Commercial MCrAlYHfSi Coating, *Surf. Coat. Technol.*, 2010, **205**, p 1178–1182

13. J. Haynes, K. Unocic, and B. Pint, Effect of Water Vapor on the 1100 °C Oxidation Behavior of Plasma-Sprayed TBCs with HVOF NiCoCrAlX Bond Coatings, *Surf. Coat. Technol.*, 2013, **215**, p 39–45

14. H.W. Grunling and R. Bauer, The Role of Silicon in Corrosion-Resistant High Temperature Coatings, *Thin Solid Films*, 1982, **95**, p 3–20

15. Q.M. Wang, Y.N. Wu, P.L. Ke, H.T. Cao, J. Gong, C. Sun, and L.S. Wen, Hot Corrosion Behavior of AIP NiCoCrAlY(SiB) Coatings on Nickel Base Superalloys, *Surf. Coat. Technol.*, 2004, **186**, p 389–397

16. N. Birks, G.H. Meier, F.S. Pettit, Introduction to the High-temperature Oxidation of Metals, 2nd ed., Cambridge University Press, 2006, pp. 111–115

17. S. Suresh, Graded Materials for Resistance to Contact Deformation and Damage, *Science*, 2001, **292**, p 2447–2451

18. X. Ren and F. Wang, High-Temperature Oxidation and Hot-Corrosion Behavior of a Sputtered NiCrAlY Coating with and Without Aluminizing, *Surf. Coat. Technol.*, 2006, **201**, p 30–37

19. M.H. Guo, Q.M. Wang, J. Gong, C. Sun, and L.S. Wen, Preparation and Oxidation of a Gradient NiCoCrAlYSiB Coating Deposited by a Combined System of Arc Ion Plating and Magnetron Sputtering, *Surf. Coat. Technol.*, 2006, **201**, p 1302–1308

20. M.H. Guo, Q.M. Wang, J. Gong, C. Sun, R.F. Huang, and L.S. Wen, Oxidation and Hot Corrosion Behavior of Gradient NiCoCrAlYSiB Coatings Deposited by a Combination of Arc Ion Plating and Magnetron Sputtering techniques, *Corros. Sci.*, 2006, **48**, p 2750–2764

21. J.R. Nicholls, N.J. Simms, W.Y. Chan, and H.E. Evans, Smart Overlay Coatings—Concept and Practice, *Surf. Coat. Technol.*, 2002, **149**, p 236–244

22. S.J. Hou, S.L. Zhu, T. Zhang, and F.H. Wang, A Magnetron Sputtered Microcrystalline β-NiAl Coating for SC Superalloys. Part I. Characterization and Comparison of Isothermal Oxidation Behavior at 1100 °C with a NiCrAlY Coating, *Appl. Surf. Sci.*, 2015, **324**, p 1–12

23. J.J. Liang, H. Wei, G.C. Hou, Q. Zheng, X.F. Sun, H.R. Guan, and Z.Q. Hu, Thermal Stability of Phases in a NiCoCrAlY Coating Alloy, *J. Mater. Res.*, 2008, **23**, p 2264–2274

24. B. Grushko, W. Kowalski, D. Pavlyuchkov, B. Przepiórzyński, and M. Surowiec, A Contribution to the Al-Ni-Cr Phase Diagram, *J. Alloy. Compd.*, 2008, **460**, p 299–304

25. C.C. Jia, K. Ishida, and T. Nishizawa, Partition of Alloying Elements Between γ (A1), γ' (L12), and β (B2) Phases in Ni-Al Base Systems, *Metall. Trans. A*, 1994, **25**, p 473–485

26. C.E. Campbell, W.J. Boettinger, and U.R. Kattner, Development of a Diffusion Mobility Database for Ni-base Superalloys, *Acta Mater.*, 2002, **50**, p 775–792

27. S. Wollmer, S. Zaefferer, M. Goken, T. Mack, and U. Glatzel, Characterization of Phases of Aluminized Nickel Base Superalloys, *Surf. Coat. Technol.*, 2003, **167**, p 83–96

28. B. Ning and M.L. Weaver, A Preliminary Study of DC Magnetron Sputtered NiAl–Hf Coatings, *Surf. Coat. Technol.*, 2004, **177–178**, p 113–120

29. N. Birks, G.H. Meier, and F.S. Pettit, *Introduction to the High-temperature Oxidation of Metals*, 2nd ed., Cambridge University Press, Cambridge, 2006, p 69–73

30. Y.F. Yang, C.Y. Jiang, H.R. Yao, Z.B. Bao, S.L. Zhu, and F.H. Wang, Cyclic Oxidation and Rumpling Behaviour of Single Phase β-(Ni, Pt)Al Coatings with Different Thickness of Initial Pt Plating, *Corros. Sci.*, 2016, **111**, p 162–174

31. H.R. Yao, Z.B. Bao, M.L. Shen, S.L. Zhu, and F.H. Wang, A Magnetron Sputtered Microcrystalline β-NiAl Coating for SC Superalloys. Part II. Effects of a NiCrO Diffusion Barrier on Oxidation Behavior at 1100 °C, *Appl. Surf. Sci.*, 2017, **407**, p 485–494

32. J.D. Nystrom, T.M. Pollock, W.H. Murphy, and A. Garg, Discontinuous Cellular Precipitation in a High Refractory Nickel Base Superalloy, *Metall. Mater. Trans. A*, 1997, **28**, p 2443–2452

33. N. Czech, F. Schmitz, and W. Stamm, Microstructural Analysis of the Role of Rhenium in Advanced MCrAlY Coatings, *Surf. Coat. Technol.*, 1995, **76–77**, p 28–33

34. W. Beele, N. Czech, W.J. Quadakkers, and W. Stamm, Long-Term Oxidation Tests on a Re-Containing MCrAlY Coatings, *Surf. Coat. Technol.*, 1997, **94–95**, p 41–45

35. O. Knotek, F. Löffler, and W. Beele, Diffusion Barrier Design Against Rapid Interdiffusion of MCrAlY and Ni-base Material, *Surf. Coat. Technol.*, 1993, **61**, p 6–13

36. L. Tianquan, G. Hongbo, P. Hui, and G. Shengkai, Precipitation Phases in the Nickel-Based Superalloy DZ 125 with YSZ/CoCrAlY Thermal Barrier Coating, *J. Alloys Comp.*, 2011, **509**, p 8542–8548

37. Y.X. Cheng, W. Wang, S.L. Zhu, L. Xin, and F.H. Wang, Arc Ion Plated-Cr_2O_3 Intermediate Film as a Diffusion Barrier Between NiCrAlY and γ-TiAl, *Intermetallics*, 2010, **18**, p 736–739

38. C.A. Guo, W. Wang, Y. Cheng, S.L. Zhu, and F.H. Wang, Yttria Partially Stabilised zirConia as Diffusion Barrier Between NiCrAlY and Ni-Base Single Crystal René N5 Superalloy, *Corros. Sci.*, 2015, **94**, p 122–128

39. M.S.A. Karunaratne, C.M.F. Rae, and R.C. Reed, On the Microstructural Instability of an Experimental Nickel-Based Single-Crystal Superalloy, *Metall. Mater. Trans.*, 2001, **32**, p 2409–2421

40. Lavigne, C. Ramusat, S. Drawin, P. Caron, D. Boivin, J.L. Pouchou, Relationships between microstructural instabilities and mechanical behaviour in new generation nickel-based single crystal superalloys, in *10th International Symposium on Superalloys, Champion, PA USA*, SEP 19–23, 2004

41. A. Sato, Y. Aoki, M. Arai, and H. Harada, Effect of Aluminizing Coating on Creep Properties of Ni-base Single Crystal Superalloys, *J. Japan Inst. Metals*, 2007, **71**, p 320–325

42. Y. Matsuoka, Y. Aoki, K. Matsumoto, A. Satou, T. Suzuki, K. Chikugo, K. Murakami, The Formation of SRZ on a Fourth Generation Single Crystal Superalloy Applied with Aluminide Coating, in *10th International Symposium on Superalloys, Champion, PA USA*, SEP 19–23, 2004

43. C.M.F. Rae, M.S. Hook, and R.C. Reed, The Effect of TCP Morphology on the Development of Aluminide Coated Superalloys, *Mater. Sci. Eng. A*, 2005, **396**, p 231–239